

See discussions, stats, and author profiles for this publication at: <https://www.researchgate.net/publication/259179109>

Examining the Effects of Different Ring Configurations and Equatorial Fluorine Atom Positions on CO₂ Sorption in [Cu(bpy)₂SiF₆]

ARTICLE in CRYSTAL GROWTH & DESIGN · AUGUST 2013

Impact Factor: 4.89 · DOI: 10.1021/cg401034s

CITATIONS

7

READS

40

8 AUTHORS, INCLUDING:



Tony Pham

University of South Florida

35 PUBLICATIONS 658 CITATIONS

[SEE PROFILE](#)



Patrick Stephen Nugent

University of South Florida

13 PUBLICATIONS 561 CITATIONS

[SEE PROFILE](#)



Brian Space

University of South Florida

91 PUBLICATIONS 1,892 CITATIONS

[SEE PROFILE](#)

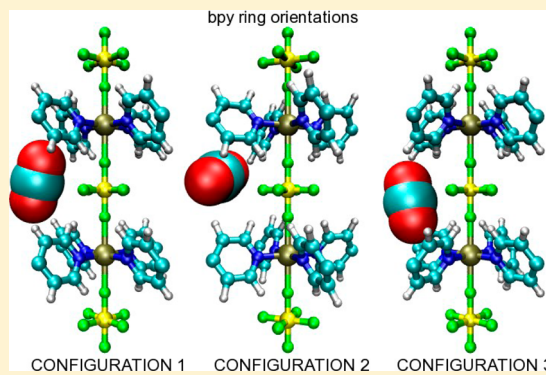
Examining the Effects of Different Ring Configurations and Equatorial Fluorine Atom Positions on CO₂ Sorption in [Cu(bpy)₂SiF₆]

Katherine A. Forrest,[§] Tony Pham,[§] Patrick Nugent, Stephen D. Burd, Ashley Mullen, Lukasz Wojtas, Michael J. Zaworotko, and Brian Space*

Department of Chemistry, University of South Florida, 4202 E. Fowler Avenue, CHE205, Tampa, Florida 33620-5250, United States

Supporting Information

ABSTRACT: Simulations of CO₂ sorption were performed in a metal–organic material (MOM) that is part of a “SIFSIX” family of compounds that has remarkable carbon dioxide capture and separation properties. The MOM considered here has the formula [Cu(bpy)₂SiF₆] (bpy = 4,4'-bipyridine). This hydrophobic MOM is both water-stable and CO₂-specific with significant sorption capacity under ambient conditions. The crystal structure reveals bpy rings and equatorial fluorine atoms in multiple possible orientations; the static disorder has been modeled based on single-crystal X-ray diffraction data revealing several possible relatives of atoms in the crystal structure. With regards to the bpy rings, the structure can be interpreted as two pyridyl rings with coplanar configurations within a unit cell (configuration 1), a twisted bpy ring conformation in which orthogonal pyridyl rings have C₄ symmetry about the Cu²⁺ ion (configuration 2), and a twisted bpy ring conformation in which the two orthogonal pyridyl rings are facing one another within a unit cell (configuration 3). Further, the equatorial fluorine atoms can be positioned such that all atoms are eclipsed with the square grid (position A), oriented at a 21.3° angle with respect to the square grid (position B), and oriented at a 45° angle with respect to the square grid (position C). It was observed that experimental data for CO₂ sorption were only consistent with sorption into configurations 1 and 3 with any of the possible equatorial fluorine atom positions at ambient temperatures, although simulations using position A produced slightly higher uptakes in these bpy ring configurations. It is demonstrated that the orientation of the bpy rings in configurations 1 and 3 allows more space for the sorbate molecules and thus promotes favorable MOM–sorbate interactions, resulting in isotherms in line with the experimental results. The results from this study suggests that [Cu(bpy)₂SiF₆] in either configuration 1 or 3 with CO₂ present in the pores at ambient temperatures is consistent with experimental sorption measurements and crystal structure data.



I. INTRODUCTION

Since pre-industrial levels, a marked ca. 43% increase in atmospheric CO₂ concentration has been observed due to the widespread use of carbonaceous fossil fuels.¹ Because these carbon-based fuels will continue to be used as our worldwide energy supply, there is an urgent demand to develop efficient carbon capture technologies in order to prevent serious environmental problems, such as global warming. Hence, research is being done to synthesize materials that can capture, separate, and store CO₂ effectively and reduce CO₂ emissions.

Metal–organic materials (MOMs) are a class of porous materials that offer great potential for applications in CO₂ storage and separations.^{2–7} These materials have been shown to store and separate CO₂ better than any porous material to date.^{2,8–12} MOMs are comprised of metal ions or metal-containing clusters with multiple points of connection and organic ligands that serve as linkers.^{13–17} They can be synthesized to have moderate to high surface areas and can be assembled from inexpensive chemicals with desired and tunable chemical functionality. A vast number of MOMs with different topologies, pore sizes, and chemical attributes have

been synthesized.¹⁷ MOMs that contain open-metal sites^{11,18} or amine functional groups^{19–21} can bind strongly to CO₂ molecules; they also have a high selectivity toward CO₂ over other gases. However, in the context of industrial gas separations, the major disadvantages of such MOMs with these features include high energy costs associated with activating and regenerating the material, high competition with water in humid environments, and stability under practical conditions.^{12,22,23}

Recently, a previously discovered class of MOMs was synthesized through a crystal engineering approach^{13,24} that does not allow open-metal sites or amine functional groups but has tailored pore sizes and displays recyclability and water stability.^{12,22,23,25–32} These MOMs are constructed with a 2D square grid based on metal ions coordinated to linear organic linkers that are pillared in the third dimension with inorganic anions to form a 3D grid that contains saturated metal centers with primitive cubic (pcu) topology. [Cu(bpy)₂SiF₆] (bpy =

Received: July 9, 2013

Published: August 26, 2013



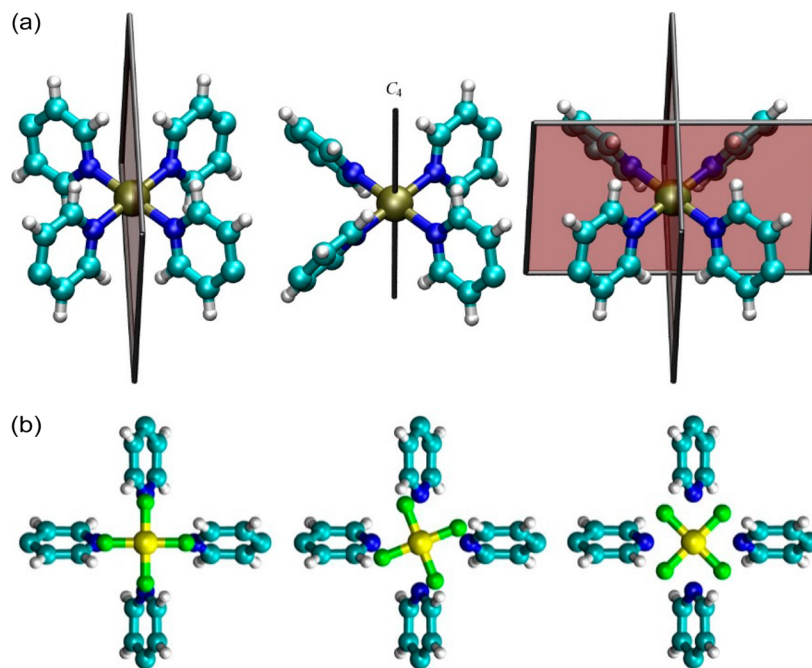


Figure 1. (a) A top view unit cell representation of the three bpy ring configurations of $[\text{Cu}(\text{bpy})_2\text{SiF}_6]$: configuration 1, where all of the bpy groups consist of the pyridyl rings in plane with each other, resulting in a single mirror plane intersecting the Cu^{2+} ion (left); configuration 2, where all the bpy groups consist of pyridyl rings that are twisted with respect to each other and where the pyridyl rings have C_4 rotational symmetry about the Cu^{2+} ion (middle); configuration 3, where the bpy groups consist of pyridyl rings that are twisted with respect to each other and where the pyridyl rings on orthogonal grids are facing toward each other, resulting in two mirror planes intersecting the Cu^{2+} (right). The SiF_6^{2-} groups are omitted for clarity. (b) A top view unit cell representation of the three equatorial fluorine atom positions of $[\text{Cu}(\text{bpy})_2\text{SiF}_6]$: position A, where the equatorial fluorine atoms are eclipsed with the pyridyl nitrogen atoms (left); position B, where the equatorial fluorine atoms are oriented at a 21.3° angle with respect to the pyridyl nitrogen atoms (middle); position C, where the equatorial fluorine atoms are oriented at a 45° angle with respect to the pyridyl nitrogen atoms (right). Atom colors: C = cyan, H = white, N = blue, F = green, Si = yellow, Cu = tan.

4,4'-bipyridine) (also known as SIFSIX-1-Cu) is a prototypical member of this family of MOMs; it consists of a 2D grid of Cu^{2+} ions that are coordinated to bpy linkers that are pillared with SiF_6^{2-} anions.^{22,26}

This MOM was initially recognized to display high uptake capacity for CH_4 .²⁶ More recently, this MOM was shown to have a high selectivity of CO_2 toward both CH_4 and N_2 at 298 K and 1.0 atm.²² As demonstrated in previous modeling studies,²³ this phenomenon can be attributed to the favorable, conformal interactions between the CO_2 molecules and the SiF_6^{2-} groups. Note that variants containing P,³¹ Ti,²³ and Sn²³ as the pillaring metal have also been synthesized.

In this study, CO_2 sorption in $[\text{Cu}(\text{bpy})_2\text{SiF}_6]$ was investigated using grand canonical Monte Carlo (GCMC) simulation methods. GCMC methods can provide atomistic detailed insights into the mechanism of gas sorption in MOMs. In addition, calculated thermodynamic observables such as isotherms and isosteric heats of adsorption, Q_{st} , can be directly compared with experimental values using this method. The agreement between experiment and simulation engenders confidence in a variety of molecular level predictions obtained from the modeling studies.

Analysis of the crystal structure of $[\text{Cu}(\text{bpy})_2\text{SiF}_6]$ reveals a number of possible configurations within the framework, particularly within the bpy rings, as well as the equatorial fluorine atoms. Three different bpy ring configurations were considered in this work (Figure 1a). Configuration 1 consists of bpy rings that are oriented such that the two pyridyl rings are in plane with one another. Configuration 2 is composed of bpy linkers in which the pyridyl rings are twisted at a 47.5° angle

and are oriented around the Cu^{2+} ion such that C_4 symmetry about the Cu–Si bond is observed. Configuration 3 is composed of bpy linkers in which the pyridyl rings are twisted at the same angle as the previous configuration but are oriented around the Cu^{2+} ion such that two mirror planes including the Cu–Si bond are observed. Moreover, the equatorial fluorine atoms of the SiF_6^{2-} groups can be positioned such that the atoms are eclipsed with the N atoms on the pyridyl rings, oriented at a 21.3° angle with respect to the N atoms, or oriented at a 45° angle with respect to the N atoms; they are denoted positions A, B, and C, respectively (Figure 1b). In essence, there are a total of nine possible configurations of $[\text{Cu}(\text{bpy})_2\text{SiF}_6]$ considered in this study. Note that only homogeneous bpy ring orientations were considered in this work. It is possible to have a mixture of coplanar and twisted bpy ring configurations within the square grid. However, we expect that the CO_2 sorption results in this configuration will be similar to that of configuration 1 because both of these configurations contain the same pyridyl ring orientations with respect to the Cu^{2+} ion.

Simulations of CO_2 sorption were performed in all considered configurations of the compound at 298 and 273 K. It will be shown that the experimental CO_2 sorption isotherms at both temperatures were reproduced for the simulations in configurations 1 and 3 for any of the possible equatorial fluorine atom positions. Note that analysis of the possible conformations of bpy in the Cu–bpy–Cu structural unit has been conducted through the search of the Cambridge Structural Database (CSD).³³ Histograms of the orientational angle demonstrate that bpy can adopt a variety of

conformations from -60 to 60° with a clear preference for 0° (coplanar rings) (see Supporting Information).

II. METHODS

For the purpose of simulation, the interactions between the MOM and the CO_2 molecules were represented by Lennard-Jones parameters (ϵ and σ), atomic point partial charges, and atomic point polarizability parameters on all atoms of the framework and the sorbate molecules. This was done to capture the corresponding van der Waals, electrostatic, and induction energetics. For $[\text{Cu}(\text{bpy})_2\text{SiF}_6]$, the Lennard-Jones parameters for all C, H, and N atoms were taken from the OPLS-AA force field,³⁴ while those for Cu, Si, and F were taken from the universal force field (UFF).³⁵ The partial charges for the atoms in $[\text{Cu}(\text{bpy})_2\text{SiF}_6]$ were obtained from periodic fitting of the entire crystal structure. More details for calculating the partial charges for the MOM atoms are provided in the Supporting Information. The polarizability parameters for C, H, N, and F were taken from van Duijnen et al.;³⁶ this set of parameters was shown to be highly transferable.^{36–44} The Cu parameter was determined in earlier work on PCN-61.⁴² The polarizability parameter for Si was determined by fitting a molecular polarizability tensor to one that was obtained from quantum mechanical calculations for gas phase SiF_6^{2-} as determined in previous work.^{23,44}

All simulations were performed in a $2 \times 2 \times 4$ unit cell system of $[\text{Cu}(\text{bpy})_2\text{SiF}_6]$ using GCMC methods. Details of the GCMC methods, including an explanation of how certain thermodynamic observables are calculated can be found in the Supporting Information. The MOM was treated as rigid during the simulations.⁴⁵ The use of a flexible force field can be executed using procedures described previously when required.^{46–48} It will be shown later that good agreement with experiment was obtained for simulations in two of the bpy ring configurations of $[\text{Cu}(\text{bpy})_2\text{SiF}_6]$ for all of the possible equatorial fluorine atom positions using a rigid model for the MOM. Thus, if the MOM was allowed to be flexible in simulation, it would be predicted that the MOM will shift toward these favorable configurations to allow for preferential interactions between the CO_2 molecules and the SiF_6^{2-} groups as explained later.

Simulations of CO_2 sorption in all configurations of $[\text{Cu}(\text{bpy})_2\text{SiF}_6]$ were performed with the inclusion of many-body polarization effects. This contribution is necessary to make favorable interactions with the polar equatorial fluorine atoms. Polarization was explicitly included in the simulations by use of a Thole–Applequist type model, which is explained in detail elsewhere^{36,37,40,42,49,50} and in the Supporting Information. A polarizable CO_2 potential energy function was used for the simulations in this work. More details of the CO_2 potential used in this study are provided in the Supporting Information and in a recent paper.⁵¹

Note, the TraPPE CO_2 model⁵² was also used as a comparison, and the results showed that it oversorbed experimental results at the temperatures investigated; these results can be found in the Supporting Information. Further, the shape of the experimental CO_2 sorption isotherms is not captured using the TraPPE model, an unsurprising result in light of the fact that this model is not parametrized for modeling interfacial interactions. TraPPE is a high fidelity condensed phase CO_2 potential that appears to not function as effectively in heterogeneous media because it is fit to function in neat CO_2 configuration space.⁵¹

III. RESULTS AND DISCUSSION

For all configurations of $[\text{Cu}(\text{bpy})_2\text{SiF}_6]$, the ground-state energy of a single unit cell was calculated for the respective structures using periodic plane-wave density functional theory (DFT) implemented on the Vienna *ab initio* simulation package (VASP)^{53–56} using the projector augmented wave (PAW) method⁵⁷ and Ceperley–Alder (CA) functional.⁵⁸ The calculations revealed that configuration 2 of the structure was the most energetically favorable configuration for the bpy ring conformations. This is true using all positions of the equatorial

fluorine atoms. For instance, the ground-state energy for configuration 2A was calculated to be -330.80 eV, whereas the energy for configuration 1A and 3A was -330.66 eV and -330.60 eV, respectively. Hence, it might be inferred that configuration 2 is the favorable bpy ring configuration for gas sorption in the MOM since it is the most stable, if the most stable crystal is formed during synthesis. However, the simulations revealed that this appears not to be the case because the theoretical results provide strong evidence for the absence of configuration 2 in the CO_2 -loaded MOM. Note, similarly, position A of the MOM was the most energetically favorable position for the equatorial fluorine atoms in all bpy ring configurations. The single-point energies for the different configurations of $[\text{Cu}(\text{bpy})_2\text{SiF}_6]$ are listed in Table 1.

Table 1. Single-Point Energies (in eV) of the Entire Unit Cell for Different Configurations of $[\text{Cu}(\text{bpy})_2\text{SiF}_6]$ as Calculated by the Vienna *ab Initio* Simulation Package (VASP)

	position A	position B	position C
configuration 1	-330.663334	-330.662387	-330.651983
configuration 2	-330.802868	-330.800069	-330.788523
configuration 3	-330.604186	-330.601639	-330.589598

Figure 2 shows the GCMC-simulated CO_2 sorption isotherms at 298 and 273 K for all configurations of $[\text{Cu}(\text{bpy})_2\text{SiF}_6]$. In configuration 2A of $[\text{Cu}(\text{bpy})_2\text{SiF}_6]$, the simulation undersorbs the experimental isotherm²² by a significant amount at all pressures at 298 K (Figure 2a). Indeed, the uptake is approximately half that of the experimental value at 298 K and 1.0 atm. Simulations in configurations 2B and 2C produced uptakes that are only marginally higher than that in configuration 2A. Analogous results can be seen for configuration 2 at 273 K (Figure 2b). In contrast, the uptakes produced in configuration 1 were significantly higher than those produced in configuration 2 for all equatorial fluorine atom positions. In configuration 1A, the simulated sorption isotherm was found to be in good agreement with the experimental isotherms at 298 K to within joint uncertainties (the maximum calculated error is ± 0.20 mmol g⁻¹). At 273 K, there is slight undersorption relative to experiment for configuration 1A, but the uptakes are still within experimental errors. Indeed, by twisting the pyridyl rings to be in the coplanar conformation, a dramatic ca. 2.50 mmol g⁻¹ increase in CO_2 uptake was observed at 1.0 atm at both temperatures. The simulated sorption isotherms for configurations 1B and 1C are slightly lower than the results for configuration 1A at both temperatures.

For configuration 3A of the MOM, the simulation predicts higher CO_2 uptakes than what was measured experimentally at 298 K; however, the generated isotherm is still within the vicinity of experiment. Further, the simulations capture good agreement with the experimental isotherm at 273 K for this configuration. Overall, by flipping the twisted pyridyl rings on one side of the square grid in configuration 2 to give rise to configuration 3, a much greater CO_2 uptake was observed. For configuration 3B, the simulation produces an isotherm that is in good agreement with experiment at both temperatures, whereas the uptakes were a little lower for simulations in configuration 3C. Note that the similarities in the results for the different equatorial fluorine atom positions in all bpy ring configurations suggest that the equatorial fluorine atoms might be in a number

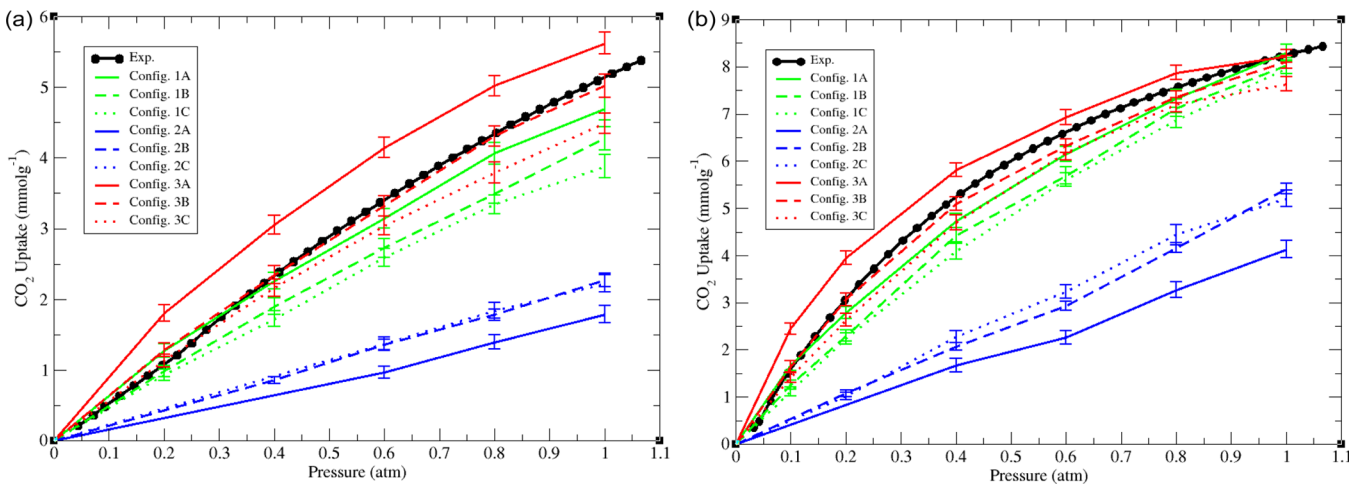


Figure 2. CO_2 sorption isotherms in $[\text{Cu}(\text{bpy})_2\text{SiF}_6]$ at (a) 298 K and (b) 273 K for experiment (black) and simulation (color). Line color indicates the bpy ring configuration in which the simulation was performed, with green corresponding to configuration 1, blue corresponding to configuration 2, and red corresponding to configuration 3. Line type indicates the equatorial fluorine atom position in which the simulation was performed, with solid corresponding to position A, dashed corresponding to position B, and dotted corresponding to position C.

of positions considering SiF_6^{2-} – CO_2 sorption in the MOM; the energy of rotation (considering barriers and minima) is also on the order of thermal motion (kT) based on VASP calculations.

The differences in uptake between the bpy ring configurations is a surprising result. It appears that small orientational changes in $[\text{Cu}(\text{bpy})_2\text{SiF}_6]$ have significant effects on the gas uptake in the compound. It is also interesting that simulations in the more energetically favorable configuration 2 failed to match the experimental isotherms at both considered temperatures. These results indicate that the presence of sorbate molecules in the MOM is consistent with configurations 1 and 3, perhaps inducing a conformational change through MOM–sorbate interactions, although these configurations might represent the MOM structure even without CO_2 present.

The GCMC-calculated Q_{st} values for $[\text{Cu}(\text{bpy})_2\text{SiF}_6]$ in all structural conformations of the MOM were examined to verify computational accuracy, and the results are shown in Figure 3. Notably, simulations in configuration 2 of the MOM showed a significant underestimation in the Q_{st} using all equatorial fluorine atom positions in comparison to the experimentally derived values that were determined using the virial method.⁵⁹ This result is consistent with the reduced accessibility of the SiF_6^{2-} group, leading to weaker MOM–sorbate interactions. On the other hand, the Q_{st} values that were produced in configurations 1 and 3 of $[\text{Cu}(\text{bpy})_2\text{SiF}_6]$ were in better agreement with experiment. Indeed, the simulation captures the experimental initial loading value in these configurations and demonstrates reasonable agreement with experiment over the range of loadings examined.

It is interesting to note that both the experimental and simulated Q_{st} values show an increase in Q_{st} for CO_2 after initial loading, a result that can be attributed to the combination of favorable MOM–sorbate and cooperative sorbate–sorbate interactions. A similar behavior was captured for a related “SIFSIX” compound in previous theoretical studies.⁴⁴ Examination of the simulation trajectories revealed a favorable sorbate–sorbate interaction between those CO_2 molecules sorbed onto neighboring equatorial fluorine atoms of the SiF_6^{2-} groups. These sorbed CO_2 molecules coordinate in a roughly slipped parallel orientation, an interaction found to be highly

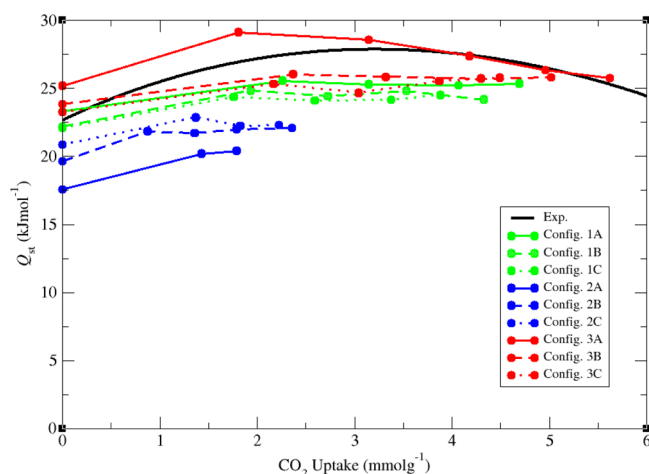


Figure 3. Isosteric heats of adsorption, Q_{st} , for CO_2 at 298 K plotted against CO_2 uptakes corresponding to pressures between 0 and 1.0 atm in $[\text{Cu}(\text{bpy})_2\text{SiF}_6]$ for experiment (black) and simulation (color). Line color indicates the bpy ring configuration in which the simulation was performed, with green corresponding to configuration 1, blue corresponding to configuration 2, and red corresponding to configuration 3. Line type indicates the equatorial fluorine atom position in which the simulation was performed, with solid corresponding to position A, dashed corresponding to position B, and dotted corresponding to position C.

favorable in CO_2 dimer interactions (see Figure S7, Supporting Information).

To understand the reason for the difference in the calculated CO_2 uptakes among all bpy ring configurations of $[\text{Cu}(\text{bpy})_2\text{SiF}_6]$, the regions of CO_2 occupancy in the respective configurations were examined via the induced dipoles resulting from the polarizable potential.^{7,23,40,42–44} Figure 4 shows the three-dimensional histogram plot within a square corridor in $[\text{Cu}(\text{bpy})_2\text{SiF}_6]$, revealing the sites of significant occupation for each of the three bpy ring configurations with position A of the equatorial fluorine atoms. The three-dimensional histogram reveals notable differences within the sorption sites among all three bpy ring configurations. It can be seen that the CO_2 molecules are closer to the equatorial fluorine atoms of the

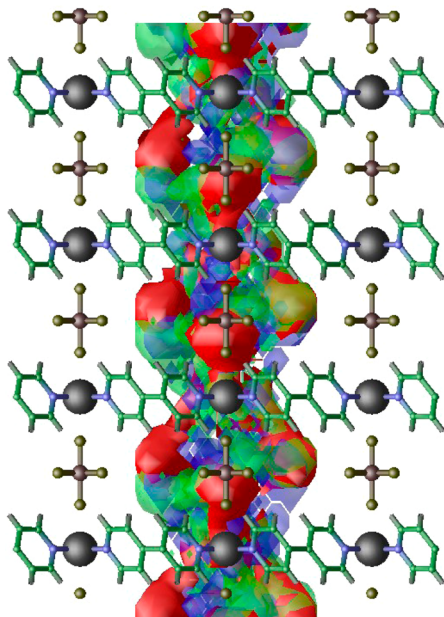


Figure 4. The three-dimensional histogram showing the sites of CO_2 sorption in all bpy ring configurations of $[\text{Cu}(\text{bpy})_2\text{SiF}_6]$ within a square corridor. The results are shown for position A of the equatorial fluorine atoms. The transparent green regions indicate occupancy for configuration 1, the transparent blue regions indicate occupancy for configuration 2, and the opaque red regions indicate occupancy for configuration 3. Atom colors: C = green, H = white, N = blue, F = yellow-green, Si = brown, Cu = black.

SiF_6^{2-} anions in configurations 1 and 3, with more occupancy being observed about the pillars in the latter configuration. In these configurations, the metal centers align with the coordinated pyridyl rings in a V-shaped orientation within the square grid, which allows the CO_2 molecules to have easy access to the equatorial fluorine atoms. Additionally, the alignment of the pyridyl rings in these configurations allows the CO_2 molecules to coordinate to two equatorial fluorine atoms simultaneously; a molecular illustration demonstrating this can

be found in Figure 5a,c. This V-shaped orientation is seen on two sides of the grid in configuration 1 and four sides of the grid in configuration 3.

The V-shaped orientation is not seen in configuration 2 due to one of the coordinated pyridyl rings being tilted in a different direction on all sides. Configuration 2 has greater relative occupation toward the center of the square pores where the MOM–sorbate interactions are weaker. In addition, as the CO_2 molecules attempt to sorb onto the equatorial fluorine atoms in this configuration, they can only do so in a sideways fashion due to blockage by one of the pyridyl rings (Figure 5b). As a result, the interaction between the CO_2 molecules and the equatorial fluorine atoms is less strong due to apparent repulsion between the electronegative oxygen and fluorine atoms. In essence, the orientation of the pyridyl rings in configuration 2 prevents significant occupancy onto the equatorial fluorine atoms. Hence, from an atomistic point of view, the observed bpy ring orientation in configuration 2 hinders sorption due to steric constraints. Note that only the results for position A in all three bpy ring configurations are described here. The results for positions B and C within the respective configurations are similar.

Though configuration 2 is consistent with the crystal structure and is the most energetically favorable configuration by a modest amount of the bpy rings in vacuum, the simulations suggest that the MOM is in either configuration 1 or 3 when the sorbate molecules are introduced with a correspondingly large sorption capacity. Indeed, the simulated CO_2 sorption isotherms are in good agreement with the experimental isotherm at both investigated temperatures when all of the pyridyl rings are in plane with one another or when all orthogonal pyridyl rings are facing toward each other. For position A of $[\text{Cu}(\text{bpy})_2\text{SiF}_6]$, configuration 2 is more stable than configurations 1 and 3 by 0.14 eV (3.23 kcal mol⁻¹) and 0.20 eV (4.61 kcal mol⁻¹), respectively. These energy differences are large enough that all the configurations would not be thermally populated under ambient conditions, but with sorbates present, the conversion is a possibility. Of course, the as-synthesized MOM is consistent with configurations 1, 2, and

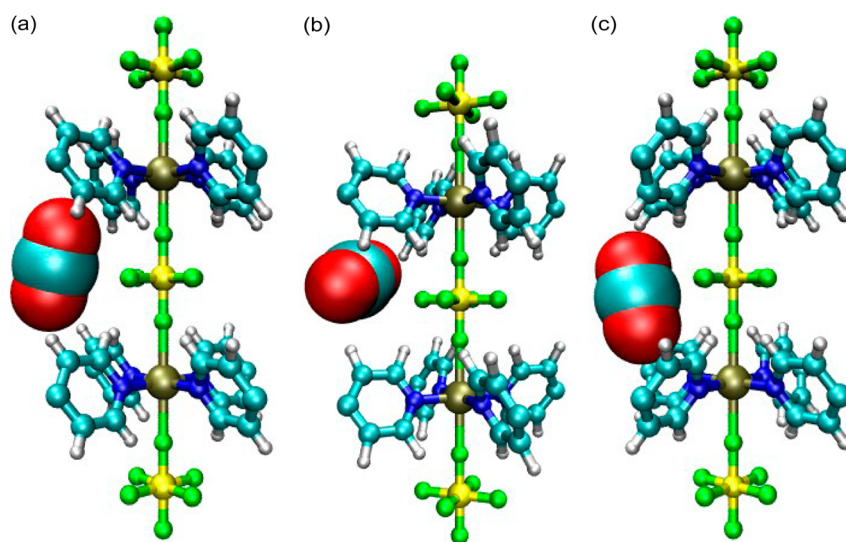


Figure 5. Molecular illustration of the CO_2 binding site about the equatorial fluorine atoms in (a) configuration 1, (b) configuration 2, and (c) configuration 3. The results are shown for position A of the equatorial fluorine atoms. Atom colors: C = cyan, H = white, N = blue, O = red, F = green, Si = yellow, Cu = tan.

3, and all are possible kinetic products. Note that the energy difference between configurations 1 and 2 agrees well with those calculated for the two conformers of 4,4'-bipyridine in vacuum.⁶⁰ Further, the low pressure region of the sorption isotherms, below one-tenth of an atmosphere, suggest that even at low loadings, configurations 1 and 3 are much better sorbents for CO₂ and that the vacuum configuration of the MOM is one of these configurations, unless an unlikely conversion takes place at very low loadings. The energy difference between configurations 1A and 3A is 0.06 eV (1.38 kcal mol⁻¹), which is small such that it would allow the configurations to interconvert between one another given the energy difference and the absence of significant barriers to conversion. In addition, with CO₂ molecules present in the MOM, both configurations 1 and 3 are possible as suggested by the simulated sorption isotherms. Note that resolving the crystal structure with sorbate molecules present might reveal the detailed nature of the structure as one of the possibilities suggested here.

IV. CONCLUSION

In conclusion, simulations of CO₂ sorption in different configurations of [Cu(bpy)₂SiF₆] were performed, and the uptakes reproduced the corresponding experimental measurements in two possible bpy ring configurations of the material suggested by the crystal structure data. Indeed, the calculated sorption isotherms for two bpy ring configurations relative to another are vastly different despite the fact that the structures are similar. Thus, this study demonstrates the ability of modeling to distinguish the differential sorption characteristics of distinct material/MOM configurations, even while constraining the MOM to be rigid. The results from this study suggest that the MOM is in the crystal configuration where the pyridyl rings of the bpy ligands are in plane with each other or twisted with each other such that the pyridyl rings on orthogonal grids are facing toward one another, at least with CO₂ gas sorbed. Note that preliminary results for CO₂ sorption in other variants of [Cu(bpy)₂MF₆], including M = Ti and Sn,²³ also show the same trends reported in this work. In addition, preliminary simulation results for CH₄, N₂, H₂, and H₂O sorption in [Cu(bpy)₂SiF₆] show the same trend as CO₂ sorption for the different configurations. Next, it is planned to simulate gas mixtures in [Cu(bpy)₂SiF₆] in an attempt to understand the mechanism of gas separations in this class of materials. The inclusion of flexibility for the simulations in this MOM would also be a task worth investigating in the future to verify the results reported herein.

■ ASSOCIATED CONTENT

Supporting Information

Details of the electronic structure calculations, tables of properties, many-body polarization overview, details of sorbate models and simulation methods, and additional content. This material is available free of charge via the Internet at <http://pubs.acs.org>.

■ AUTHOR INFORMATION

Corresponding Author

*E-mail: brian.b.space@gmail.com.

Author Contributions

[§]K.A.F. and T.P. contributed equally.

Notes

The authors declare no competing financial interest.

■ ACKNOWLEDGMENTS

This work was supported by the National Science Foundation (Award No. CHE-1152362). Computations were performed under a XSEDE Grant (No. TG-DMR090028) to B.S. This publication is also based on work supported by Award No. FIC/2010/06, made by King Abdullah University of Science and Technology (KAUST). The authors also thank the Space Foundation (Basic and Applied Research) for partial support. The authors acknowledge the use of the services provided by Research Computing at the University of South Florida.

■ REFERENCES

- (1) Carbon dioxide passes symbolic mark. 2013; <http://www.bbc.co.uk/news/science-environment-22486153>. Accessed June 26, 2013.
- (2) Sumida, K.; Rogow, D. L.; Mason, J. A.; McDonald, T. M.; Bloch, E. D.; Herm, Z. R.; Bae, T.-H.; Long, J. R. *Chem. Rev.* **2012**, *112*, 724–781.
- (3) Snurr, R. Q.; Hupp, J. T.; Nguyen, S. T. *AIChE J.* **2004**, *50*, 1090–1095.
- (4) Delgado, J. A.; Uguina, M. A.; Gmez, J. M.; Ortega, L. *Sep. Purif. Technol.* **2006**, *48*, 223–228.
- (5) Babarao, R.; Eddaoudi, M.; Jiang, J. W. *Langmuir* **2010**, *26*, 11196–11203.
- (6) Li, J.-R.; Ma, Y.; McCarthy, M. C.; Sculley, J.; Yu, J.; Jeong, H.-K.; Balbuena, P. B.; Zhou, H.-C. *Coord. Chem. Rev.* **2011**, *255*, 1791–1823.
- (7) Mohamed, M. H.; Elsaiedi, S. K.; Wojtas, L.; Pham, T.; Forrest, K. A.; Tudor, B.; Space, B.; Zaworotko, M. J. *J. Am. Chem. Soc.* **2012**, *134*, 19556–19559.
- (8) Millward, A. R.; Yaghi, O. M. *J. Am. Chem. Soc.* **2005**, *127*, 17998–17999 PMID: 16366539.
- (9) Banerjee, R.; Phan, A.; Wang, B.; Knobler, C.; Furukawa, H.; O'Keeffe, M.; Yaghi, O. M. *Science* **2008**, *319*, 939–943.
- (10) Caskey, S. R.; Wong-Foy, A. G.; Matzger, A. J. *J. Am. Chem. Soc.* **2008**, *130*, 10870–10871 PMID: 18661979.
- (11) Britt, D.; Furukawa, H.; Wang, B.; Glover, T. G.; Yaghi, O. M. *Proc. Natl. Acad. Sci. U. S. A.* **2009**, *106*, 20637–20640.
- (12) Nugent, P.; Belmabkhout, Y.; Burd, S. D.; Cairns, A. J.; Lue-bke, R.; Forrest, K.; Pham, T.; Ma, S.; Space, B.; Wojtas, L.; Eddaoudi, M.; Zaworotko, M. J. *Nature* **2013**, *495*, 80–84.
- (13) Moulton, B.; Zaworotko, M. J. *Chem. Rev.* **2001**, *101*, 1629–1658.
- (14) Yaghi, O. M.; Li, H.; Davis, C.; Richardson, D.; Groy, T. L. *Acc. Chem. Res.* **1998**, *31*, 474–484.
- (15) Eddaoudi, M.; Moler, D. B.; Li, H.; Chen, B.; Reineke, T. M.; O'Keeffe, M.; Yaghi, O. M. *Acc. Chem. Res.* **2001**, *34*, 319–330 PMID: 11308306.
- (16) Eddaoudi, M.; Kim, J.; Rosi, N.; Vodak, D.; Wachter, J.; O'Keeffe, M.; Yaghi, O. M. *Science* **2002**, *295*, 469–472.
- (17) Eddaoudi, M.; Eubank, J. F. *Metal-Organic Frameworks*; John Wiley & Sons, Inc.: Hoboken, NJ, 2010; pp 37–89.
- (18) Chen, B.; Ockwig, N. W.; Millward, A. R.; Contreras, D. S.; Yaghi, O. M. *Angew. Chem.* **2005**, *117*, 4823–4827.
- (19) Li, B.; et al. *Angew. Chem., Int. Ed.* **2012**, *51*, 1412–1415.
- (20) Lin, J.-B.; Zhang, J.-P.; Chen, X.-M. *J. Am. Chem. Soc.* **2010**, *132*, 6654–6656.
- (21) Lin, Q.; Wu, T.; Zheng, S.-T.; Bu, X.; Feng, P. *J. Am. Chem. Soc.* **2012**, *134*, 784–787.
- (22) Burd, S. D.; Ma, S.; Perman, J. A.; Sikora, B. J.; Snurr, R. Q.; Thallapally, P. K.; Tian, J.; Wojtas, L.; Zaworotko, M. J. *J. Am. Chem. Soc.* **2012**, *134*, 3663–3666.
- (23) Nugent, P.; Rhodus, V.; Pham, T.; Tudor, B.; Forrest, K.; Wojtas, L.; Space, B.; Zaworotko, M. *Chem. Commun.* **2013**, *49*, 1606–1608.
- (24) Desiraju, G. *Angew. Chem., Int. Ed.* **2007**, *46*, 8342–8356.

- (25) Subramanian, S.; Zaworotko, M. J. *Angew. Chem., Int. Ed. Engl.* **1995**, *34*, 2127–2129.
- (26) Noro, S.-i.; Kitagawa, S.; Kondo, M.; Seki, K. *Angew. Chem., Int. Ed.* **2000**, *39*, 2081–2084.
- (27) Uemura, K.; Maeda, A.; Maji, T. K.; Kanoo, P.; Kita, H. *Eur. J. Inorg. Chem.* **2009**, *2009*, 2329–2337.
- (28) Lin, M.-J.; Jouaiti, A.; Kyritsakas, N.; Hosseini, M. W. *CrystEngComm* **2011**, *13*, 776–778.
- (29) Lin, M.-J.; Jouaiti, A.; Kyritsakas, N.; Hosseini, M. W. *CrystEngComm* **2009**, *11*, 189–191.
- (30) Kanoo, P.; Reddy, S. K.; Kumari, G.; Haldar, R.; Narayana, C.; Balasubramanian, S.; Maji, T. K. *Chem. Commun.* **2012**, *48*, 8487–8489.
- (31) Noro, S.-i.; Hijikata, Y.; Inukai, M.; Fukushima, T.; Horike, S.; Higuchi, M.; Kitagawa, S.; Akutagawa, T.; Nakamura, T. *Inorg. Chem.* **2013**, *52*, 280–285.
- (32) Xiong, S.; He, Y.; Krishna, R.; Chen, B.; Wang, Z. *Cryst. Growth Des.* **2013**, *13*, 2670–2674.
- (33) Allen, F. H. *Acta Crystallogr., Sect. B: Struct. Sci.* **2002**, *58*, 380–388.
- (34) Jorgensen, W. L.; Maxwell, D. S.; Tirado-Rives, J. *J. Am. Chem. Soc.* **1996**, *118*, 11225–11236.
- (35) Rappe, A. K.; Casewit, C. J.; Colwell, K. S.; Goddard, W. A.; Skiff, W. M. *J. Am. Chem. Soc.* **1992**, *114*, 10024–10035.
- (36) van Duijnen, P. T.; Swart, M. *J. Phys. Chem. A* **1998**, *102*, 2399–2407.
- (37) Applequist, J.; Carl, J. R.; Fung, K.-K. *J. Am. Chem. Soc.* **1972**, *94*, 2952–2960.
- (38) DeVane, R.; Space, B.; Perry, A.; Neipert, C.; Ridley, C.; Keyes, T. *J. Chem. Phys.* **2004**, *121*, 3688–3701.
- (39) Perry, A.; Neipert, C.; Space, B.; Moore, P. B. *Chem. Rev.* **2006**, *106*, 1234–1258 PMID: 16608179.
- (40) Belof, J. L.; Stern, A. C.; Eddaoudi, M.; Space, B. *J. Am. Chem. Soc.* **2007**, *129*, 15202–15210 PMID: 17999501.
- (41) Stern, A. C.; Belof, J. L.; Space, B. *J. Phys. Chem. C* **2012**, *136*, No. 034705.
- (42) Forrest, K. A.; Pham, T.; McLaughlin, K.; Belof, J. L.; Stern, A. C.; Zaworotko, M. J.; Space, B. *J. Phys. Chem. C* **2012**, *116*, 15538–15549.
- (43) Pham, T.; Forrest, K. A.; Nugent, P.; Belmabkhout, Y.; Luebke, R.; Eddaoudi, M.; Zaworotko, M. J.; Space, B. *J. Phys. Chem. C* **2013**, *117*, 9340–9354.
- (44) Pham, T.; Forrest, K. A.; McLaughlin, K.; Tudor, B.; Nugent, P.; Hogan, A.; Mullen, A.; Cioce, C. R.; Zaworotko, M. J.; Space, B. *J. Phys. Chem. C* **2013**, *117*, 9970–9982.
- (45) Greathouse, J. A.; Allendorf, M. D. *J. Phys. Chem. C* **2008**, *112*, 5795–5802.
- (46) Grosch, J. S.; Paesani, F. *J. Am. Chem. Soc.* **2012**, *134*, 4207–4215.
- (47) Cirera, J.; Sung, J. C.; Howland, P. B.; Paesani, F. *J. Chem. Phys.* **2012**, *137*, 054704.
- (48) Paesani, F. *Mol. Simul.* **2012**, *38*, 6311.
- (49) Thole, B. *Chem. Phys.* **1981**, *59*, 341–350.
- (50) Bode, K. A.; Applequist, J. *J. Phys. Chem.* **1996**, *100*, 17820–17824.
- (51) Mullen, A.; Pham, T.; Forrest, K. A.; Cioce, C. R.; McLaughlin, K.; Space, B. *J. Chem. Theory Comput.* **2013**, submitted for publication.
- (52) Potoff, J. J.; Siepmann, J. I. *AIChE J.* **2001**, *47*, 1676–1682.
- (53) Kresse, G.; Hafner, J. *Phys. Rev. B* **1993**, *47*, 558–561.
- (54) Kresse, G.; Hafner, J. *Phys. Rev. B* **1994**, *49*, 14251–14269.
- (55) Kresse, G.; Furthmüller, J. *Comput. Mater. Sci.* **1996**, *6*, 15–50.
- (56) Kresse, G.; Furthmüller, J. *Phys. Rev. B* **1996**, *54*, 11169–11186.
- (57) Blochl, P. E. *Phys. Rev. B* **1994**, *50*, 17953.
- (58) Ceperley, D. M.; Alder, B. *J. Phys. Rev. Lett.* **1980**, *45*, 566–569.
- (59) Dinca, M.; Dailly, A.; Liu, Y.; Brown, C. M.; Neumann, D. A.; Long, J. R. *J. Am. Chem. Soc.* **2006**, *128*, 16876–16883 PMID: 17177438.
- (60) Pérez-Jiménez, Á. J.; Sancho-García, J. C.; Pérez-Jordá, J. M. *J. Chem. Phys.* **2005**, *123*, No. 134309.